 

PACS numbers: 52.50.Jm; 42.65.Re; 42.70.Ce
DOI: 10.1070/QE2012v042n10ABEH014895

# Femtosecond laser pulse filamentation under anomalous dispersion in fused silica. Part 1. Numerical investigation

E.O. Smetanina, V.O. Kompanets, S.V. Chekalin, V.P. Kandidov

*Abstract.* **We report the results of investigation of femtosecond laser pulse filamentation in fused silica by varying the wavelength in the range from 800 to 2300 nm. It is shown that in the case of the anomalous group-velocity dispersion, a sequence of 'light bullets' with a high spatial and temporal localisation of the light field is formed along the filament. The relation of the formation and propagation of light bullets with the formation of an isolated anti-Stokes wing of the supercontinuum spectrum is established.**

***Keywords:*** *filamentation, supercontinuum generation, light bullets.*

## 1. Introduction

Transformation of the spatiotemporal intensity distribution and frequency-angular spectrum of a femtosecond pulse during filamentation in condensed media has been studied in many papers [1–4]. Based on these studies, methods for pulse compression and broadband supercontinuum (SC) generation are being developed. Changing the shape and spectrum of the pulse during filamentation is the result of the joint influence of strong nonlinear-optical interaction of laser pulses with the medium and of the effects of wave dispersion and diffraction. In condensed media, material dispersion affects dramatically the transformation of the pulse shape. Under conditions of the normal group-velocity dispersion (GVD), the pulse is split into subpulses having different group velocities, the distance between the subpulses increasing during their propagation in a dispersive medium [5, 6]. In the case of the anomalous GVD under conditions of self-phase modulation, the light field 'contracts' to the centre of the pulse [7, 8]. However, according to the numerical simulation [9], the super-Gaussian pulses, in contrast to Gaussian ones, split into subpulses in the anomalous GVD regime.

The length of the filament in the case of the anomalous GVD is much longer than that in the case of the normal GVD [10]. In the anomalous GVD, the radiation beam, whose power is a thousand times greater than the critical self-focusing power, splits into multiple filaments, in which the pulse duration is compressed [11]. Liu et al. [12] showed numerically that the spatiotemporal dynamics of the pulse shape at the centre wavelength of $\lambda_0 = 800$ nm in the region of the normal GVD in fused silica leads to the formation of an X-wave, whereas at the wavelength of $\lambda_0 = 1600$ nm the light pulse in the region of the anomalous GVD is transformed into a few-cycle spatiotemporal wave soliton. According to the numerical study of the filamentation process of 1550-nm pulsed radiation in fused silica, in the fifth-order dispersion approximation [7] a quasi-periodic sequence of spatiotemporal localisations of a few-cycle light field is formed in the case of the anomalous GVD.

An important manifestation of spatiotemporal pulse transformation is the generation of a coherent SC, i.e., the broadening of the pulse spectrum, during which its spectral width becomes comparable to the fundamental frequency of radiation [1–3, 13]. The first experiments on generation of broadband radiation were performed by focusing laser pulses (530 nm, 4 ps and 5 GW) in condensed media (calcite, silica, sodium chloride and glass) [14]. In all the materials the frequency shift to the anti-Stokes region exceeded the Stokes shift. Bondarenko et al. [14] explained that the generation of broadband radiation was due to the laser pulse self-phase modulation under conditions of electronic Kerr nonlinearity. In experiments performed in various condensed media, Brodeur and Chin [15] found that for femtosecond laser pulses ($\lambda_0 = 796$ nm) and a medium band gap that is less than a certain threshold value the SC generation is absent. This threshold is determined by the condition $U_i/(\hbar\omega_0) > 2$, where $U_i$ is the band gap of the material, and $\omega_0$ is the radiation frequency. In this case, the width of the anti-Stokes band of the SC increases with increasing material band gap that exceeds a threshold value. Based on the experiments with femtosecond pulse ($\lambda_0 = 785$, 393 and 262 nm) filamentation in various optical materials, the general principle has been formulated that the broadening of the SC spectrum to the blue region does not depend on the parameters of the medium and laser pulse, but only on the ratio $U_i/(\hbar\omega_0)$, thereby increasing with its increase [16]. In this case, the anti-Stokes broadening is independent of the laser pulse intensity [17].

In the normal GVD, according to the experiments [18] on filamentation of a 810-nm laser pulse in fused silica, the intensity of the spectral components in the anti-Stokes band decreases monotonically with increasing detuning of their wavelengths from the centre wavelength. A monotonic decrease in the intensity of the spectral SC components with detuning of their wavelength both in the Stokes and anti-Stokes regions of the spectrum was recorded in the filamentation of pulses with the energies of 0.4–200 μJ in water, chlo-

**E.O. Smetanina, V.P. Kandidov** Department of Physics, M.V. Lomonosov Moscow State University, Vorov'evy gory, 119991 Moscow, Russia; e-mail: smetanina@physics.msu.ru, kandidov@physics.msu.ru;
**V.O. Kompanets, S.V. Chekalin** Institute of Spectroscopy, Russian Academy of Sciences, ul. Fizicheskaya 5, 142190 Troitsk, Moscow region, Russia; e-mail: kompanetsvo@isan.troitsk.ru, chekalin@isan.troitsk.ru

Received 14 May 2012; revision received 12 July 2012
*Kvantovaya Elektronika* **42** (10) 913–919 (2012)
Translated by I.A. Ulitkin

roform and glass at $\lambda_0 = 810$ nm [17], as well as in various laser materials (YAG, sapphire, KGW, $YVO_4$ and $GdVO_4$) at $\lambda_0 = 775$ nm [19]. To this end, monotonous broadening of the spectrum to the blue region up to 530 nm was observed in the YAG crystal at $\lambda_0 = 1100-1600$ nm.

However, there are a number of works where the SC spectra with a nonmonotonic blue region were observed during filamentation in condensed media. A nonmonotonic dependence of the intensity of the anti-Stokes components on the wavelength was recorded in $BaF_2$ crystals at $\lambda_0 = 800$ nm with increasing peak power up to $1000P_{cr}$ ($P_{cr}$ is the critical self-focusing power) [20] and in LiF crystals with increasing peak intensity up to 30 TW cm$^{-2}$ [21]. During filamentation of a femtosecond pulse in the region of the anomalous GVD in fused silica ($\lambda_0 = 1500$ nm), Saliminia et al. [22] have registered a broad maximum in the vicinity of $\lambda \simeq 600$ nm, which extends from 400 to 1000 nm in the anti-Stokes region of the SC. Saliminia et al. [22] point to the fact that a 'dip' in the spectral components the SC is formed in the region of the zero GVD in fused silica. The peak in the visible SC spectrum was recorded in multiple filamentation of 100-GW pulses at $\lambda_0 = 1540$ nm in fused silica [23]. The maximum of the spectral intensity at $\lambda = 670$ nm in the anti-Stokes region of the SC during filamentation of 1600-nm pulses in fused silica was obtained numerically in [12].

In this paper we have studied the features of transformation of the shape and spectrum of femtosecond laser pulses during filamentation in fused silica under conditions of the anomalous GVD. We present the results of numerical simulation of filamentation of a femtosecond pulse with a centre wavelength tunable in the range of 800–2300 nm, which corresponds to the normal, zero, and anomalous GVD.

## 2. Mathematical model of femtosecond pulse filamentation in fused silica

To study numerically the spatiotemporal and spectral transformation of a femtosecond pulse in fused silica, we used the slowly-evolving-wave approximation [24], which the authors called the method of a slowly varying wave. According to this method, the equation in the moving coordinate system for the complex field amplitude $A(r,t,z)$ at a carrier frequency $\omega_0$ has the form

$$2ik_0\frac{\partial A(r,t,z)}{\partial z} = \hat{T}^{-1}\Delta_\perp A(r,t,z) + \int_{-\infty}^{\infty}\frac{1}{1+\Omega/\omega_0}$$

$$\times[k^2(\omega_0+\Omega)-(k_0+k'_\omega\,\Omega)^2]\tilde{A}(r,\Omega,z)e^{i\Omega t}d\Omega$$

$$+\frac{2k_0^2}{n_0}\hat{T}[\Delta n_K(r,t,z)]+\frac{2k_0^2}{n_0}\hat{T}^{-1}[\Delta n_p(r,t,z)A(r,t,z)]$$

$$-ik_0\hat{T}^{-2}[\sigma N_e(r,t,z)A(r,t,z)]-ik_0\alpha(r,t,z)A(r,t,z), \quad (1)$$

where $\tilde{A}(r,\Omega,z)$ is the time Fourier transform of the envelope; $\Omega = \omega - \omega_0$ is the shift of the frequency in the harmonic pulse spectrum at a frequency $\omega$ from the centre frequency $\omega_0$; $k_0 = \omega_0 n(\omega_0)/c_0$ is the wave number; $c_0$ is the speed of light; and $n_0 \approx 1.45$ is the refractive index of fused silica. The dependence $k(\omega) = \omega n(\omega)/c_0$ and the parameter $k'_\omega = \partial k/\partial\omega\big|_{\omega=\omega_0}$ with the function $n(\omega)$, approximated by the Sellmeier formula [25], describe the material dispersion in fused silica. The operator $\hat{T} = 1 - (i/\omega_0)\partial/\partial t$ makes it possible to reproduced the wave nonstationary behaviour upon pulse self-modulation, which results in increasing the steepness of the trailing edge of the pulse (so0called self-steepening effect) and in forming the shock wave of the envelope [26]. The refractive index increment $\Delta n_K(r,t,z)$, due to the Kerr nonlinearity of the medium, is represented as a convolution [27]:

$$\Delta n_K(r,t,z) = n_2\left[(1-g)I(r,t,z) + g\int_{-\infty}^{t}h(1-\tau)I(r,t,z)d\tau\right], \quad (2)$$

where $I(r,t,z)$ is the intensity of the light field; $n_2 \approx 3.54\times10^{-16}$ cm$^2$ W$^{-1}$ is the Kerr nonlinearity coefficient for the quasi-stationary radiation [25, 28]; and g = 0.18 is the partial contribution of the Raman response. The function of a delayed nonlinear response [25] is

$$h(t) = \frac{\tau_1^2+\tau_2^2}{\tau_1^2\tau_2}\exp\left(-\frac{t}{\tau_1}\right)\sin\left(\frac{t}{\tau_2}\right),\ \tau_1 = 32\text{ fs},\ \tau_2 = 12.5\text{ fs}. \quad (3)$$

The nonlinearity $\Delta n_p$ and bremsstrahlung cross section $\sigma$ of the light field in the plasma are given by

$$\Delta n_p(r,t,z) = -\frac{4\pi e^2 N_e(r,t)}{2n_0\omega_0^2 m_e}, \quad (4)$$

$$\sigma = \frac{k_0 4\pi e^2}{n_0^2\omega_0^2 m_e}\frac{\nu_c}{\omega_0}, \quad (5)$$

where $\nu_c \approx 10^{14}$ s$^{-1}$ is the rate of electron–ion collisions, and $m_e$ and $e$ are the electron mass and charge. The concentration of free electrons in the laser plasma, $N_e$, obeys the kinetic equation

$$\frac{\partial N_e}{\partial t} = W(I)(N_0 - N_e) + \nu_i N_e, \quad (6)$$

where $N_0$ is the concentration of neutral atoms (for silica $N_0 = 2\times10^{22}$ cm$^{-3}$); $W(I)$ is the rate of field ionisation, defined by the Keldysh formula [29]; and

$$\nu_i = \frac{e^2|A|^2}{2U_i m_e(\omega_0^2+\nu_c^2)}\nu_c \quad (7)$$

is the frequency of avalanche ionisation. The band gap for fused silica is $U_i \approx 9$ eV. For 800-nm radiation with an intensity of $I \sim 10^{14}$ W cm$^{-2}$, which is characteristic of the filamentation regime, the frequency $\nu_i \approx 10^{14}$ s$^{-1}$, and the avalanche ionisation makes a significant contribution to the increase in the electron density of a femtosecond pulse. Equation (6) does not take into account the recombination of electrons, the typical time of which is a few hundred femtoseconds. The decay of the light field is determined by the losses to generate the laser plasma

$$\alpha = \frac{K\hbar\omega_0}{I}W(I)(N_0 - N_e), \quad (8)$$

where $K = [U_i/(\hbar\omega_0)+1]$ is the multiphoton order of the ionisation process.

The input pulse had the form of a transform-limited pulse with a Gaussian distribution of the field amplitude in space and time:

$$A(r,t,z=0) = A_0\exp\left(-\frac{r^2}{2a_0^2}-\frac{r^2}{2\tau_0^2}\right), \quad (9)$$

where $a_0$ is the beam radius and $\tau_0$ is the parameter determining the pulse duration. We considered the system of equations (1)–(8) with condition (9) in an axisymmetric formulation.

The numerical simulation made it possible to find the distribution of the complex amplitude, $A(r,t,z)$, and the electron density in self-induced laser plasma, $N_e(r,t,z)$, with respect to time $t$ and spatial coordinates $r,z$. In addition, we calculated the intensity of the spectral components in the cross section plane

$$S(r,\omega,z) = \text{const}\left|\int_{-\infty}^{\infty} A(r,z,t)\mathrm{e}^{-\mathrm{i}\Omega t}\mathrm{d}t\right|^2$$

and the spectral density of the SC power

$$S(\omega,z) = \text{const}\int_0^{\infty} S(r,\omega,z)\mathrm{d}r. \qquad (10)$$

The computed pulse spectrum $S_{\text{comp}}(\lambda,z)$, similar to that obtained in a physical experiment, has the form

$$S_{\text{comp}}(\lambda,z) = S(\omega(\lambda),z)\frac{2\pi c_0 n(\lambda)}{\lambda^2}. \qquad (11)$$

The scenario of femtosecond laser pulse filamentation is determined by a number of factors, such as the Kerr self-focusing and self-modulation, intensity clamping and defocusing of the pulse tail in laser plasma, and finally the wave processes of diffraction and dispersion of the pulse in the medium. In terms of numerical simulation, the SC generation is a multiparameter problem whose analysis on the entire set of physical parameters is very complex and not very productive at the same time. In this regard, we performed a series of numerical experiments for pulses with a centre wavelength tunable in the range of $\lambda_0 = 800-2300$ nm, for equal values of similarity parameters that define the initial stage of filamentation due to the Kerr self-focusing. These parameters are the diffraction length $L_d = ka_0^2$ and the ratio of the peak power, $P$, to the critical power, $P_{cr}$. The values of the beam radius are taken equal to several tens of micrometres, which is similar to those used in the laboratory experiment [8, 30]. In the entire range of wavelengths, the diffraction length of the beam is $L_d \approx 3$ cm and the peak power is $P = 5P_{cr}$, which corresponds to the regime of one filament. The pulse duration $2\tau_0$ at the 1/e level was 80 fs, which corresponds to the FWHM pulse duration $\tau_p = 70$ fs.

Thus, the conditions for the propagation of a pulse in a medium to the nonlinear focus plane, where plasma is produced, differ only by the influence of the GVD, which is dependent on the wavelength. In the nonlinear focus, generation of the laser plasma limits the growth of the intensity during self-focusing, which is determined by the multiphoton order $K$, which ranges from 6 for $\lambda_0 = 800$ nm to 17 for $\lambda_0 = 2300$ nm. In this formulation of the problem, it is possible to isolate the effect of the wavelength on the spatiotemporal and spectral transformation of radiation, which involves the influence of the GVD, formation of a shock wave, and the SC generation.

## 3. 'Light bullets' and the SC spectrum in the filament

Consider spatiotemporal and spectral transformation of pulsed radiation with the centre wavelength $\lambda_0 = 1900$ nm, energy $W = 3.77$ μJ and peak intensity $I_0 = 2.7\times10^{11}$ W cm$^{-2}$. For this wavelength the GVD in fused silica is anomalous, and the parameter $k_2$ determining the change in the pulse duration due to the GVD is equal to –23 fs$^2$ cm$^{-1}$. During femtosecond laser pulse filamentation, the light field is quasi-periodically localised in space and time, resulting in a sequence of light bullets along the direction of its propagation (Fig. 1). The peak intensity in the light bullet increases hundreds of times and reaches $5.2\times10^{13}$ W cm$^{-2}$, the radius (in intensity) of its cross section is ~6 μm, and the duration is a few field oscillation cycles. The light bullet is formed in the central time layers of the pulse, where the intensity is maximal. Further propagation in silica causes the light bullet to move to the pulse tail, and its peak intensity decreases. The movement of the bullet to the tail of the pulse is accompanied by re-localisation of the light field due to self-focusing in the central time layers, and a new bullet is formed. This cycle of generation of light bullets in the centre of the pulse is repeated many times, because in the case of the anomalous GVD the power 'flows' to the centre from the tail and the leading edge of the pulse. The number of bullets, the generation of which is maintained by the anomalous GVD, increases with increasing pulse intensity.

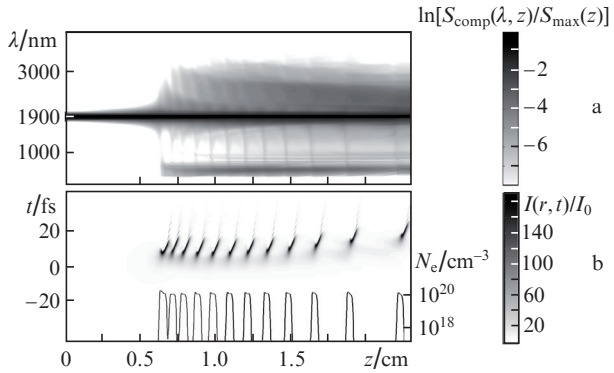


**Figure 1.** Tone images of transformations of the normalised (a) pulse spectrum $S_{comp}(\lambda,z)/S_{max}(z)$ and (b) pulse shape on the axis $I(r=0,t,z)/I_0$ with distance $z$. At the bottom of panel (b) the distribution of the electron concentration of the laser plasma, $N_e(z)$, on the axis is shown. The centre wavelength is $\lambda_0 = 1900$ nm, the peak power is $P = 53$ MW ($P = 5P_{cr}$), the pulse duration (at e$^{-1}$ level) is $2\tau_0 = 80$ fs and the beam radius is $a_0 = 80$ μm.

Before the formation of the light bullets, the pulse spectrum $S_{comp}(\lambda)$ monotonically and symmetrically broadens relative to the centre wavelength $\lambda_0$. The emergence of each light bullet with a high energy density is closely related to the generation of laser plasma and a strong self-phase modulation of the light field, which causes the broadening of the spectrum (Fig. 1). Therefore, the position and extent of plasma channels coincide with the regions of formation of light bullets, which can be defined as emitting SC regions in the filament. At a distance $z$, where a new light bullet emerges, there occurs generation of the SC whose spectrum extends into the anti-Stokes (blue) region up to $\lambda = 300$ nm. In this case, the SC spectrum $S_{comp}(\lambda)$, which is generated by each bullet at the place of its formation, is monotonically and symmetrically broadened relative to the centre wavelength.

In Fig. 1, the spectrum broadening, calculated at the point of formation of light bullets, is seen by thin lines between the centre wavelength of 1900 nm and anti-Stokes region. A sharp increase in the width of the spectrum, corresponding to the formation of a next light bullet, is clearly seen in the range from 0.95 to 1.75 cm. When the light bullet propagates and then disappears, a minimum of width ~1000 nm is formed in the spectrum $S_{comp}(\lambda)$, which separates the central part of the

spectrum and the anti-Stokes (blue) wing, which lies in the vicinity of $\lambda = 600$ nm. The intensity of spectral components of the anti-Stokes wing increases with increasing number of the bullets produced, and the interference maxima appear in the spectrum.

To analyse the effect of the wavelength of the input pulse, $\lambda_0$, on the formation of the SC spectrum $S_{comp}(\lambda_0, \lambda)$, we performed a series of numerical experiments on filamentation of laser pulses with $\lambda_0$, varied in the range from 800 to 2300 nm. The results obtained numerically are summarised in Figs 2 and 3 in the form of a spectral SC map, in which the intensity of its spectral components is presented by the surface on the plane with the coordinates $\lambda$, $\lambda_0$. In these figures, the global maximum of the surface, $S_{comp}(\lambda_0, \lambda)$, which corresponds to a component at the centre wavelength $\lambda_0$ in the spectrum, lies on the bisector shown by a thin dashed line. The intensities of the spectral components of the SC are normalised to the maximum value $S_{max\,\lambda_0}$ for each centre wavelength. In the logarithmic scale, the global maximum on the spectral map $S_{comp}(\lambda_0, \lambda)/S_{max\,\lambda_0}$ is zero.

In constructing the SC map, we used the spectra $S_{comp}(\lambda_0,\lambda)$, which are formed in the filament at a distance $z(\lambda_0)$, typical of the pulse with the centre wavelength $\lambda_0$. Figure 2a shows the spectral map $S_{comp}(\lambda_0,\lambda)$ for those distances at which a nonlinear focus emerges and the first light bullet begins to form during filamentation of the laser pulse with the wavelength $\lambda_0$. At these distances, the SC source can be considered as a point source. Figure 2b–d present the spatiotemporal distributions of the intensity $I(r,t)$ and the pulse profiles on the axis $I(r = 0,t)$ at a zero GVD and $\lambda_0 = 1300$ nm, and at an anomalous GVD and $\lambda_0 = 1900$ and 2100 nm. The SC spectra $S_{comp}(\lambda)$ for the incident pulse at these wavelengths are shown by dashed white lines on the spectral map. It is seen that in the nonlinear focus the pulse spectrum broadens monotonically from the centre wavelength $\lambda_0$ both in the Stokes (red) and anti-Stokes (blue) regions. The spectrum broadening is the result of self-phase modulation of the light field in the filament. In this case, the anti-Stokes broadening is due to the self-phase modulation at the pulse tail, where the self-steepening of the envelope plays an important role. In Fig. 2, an increase in the slope of the trailing edge of the pulse is illustrated by the profiles $I(r = 0,t)$. The self-steepeing of the trailing edge of the pulse strongly increases with increasing centre wavelength $\lambda_0$. The time intensity gradient in the pulse tail increases and anti-Stokes spectral broadening turns to be much larger than that for the zero GVD. It should be noted that the highest peak intensity both in units of $I_0$ and in absolute units (W cm$^{-2}$) is achieved in filamentation of a 1300-nm pulse, the conditions corresponding to the zero GVD. However, the slope of the trailing edge of the pulse and, therefore, the anti-Stokes broadening of the SC is much less at the zero GVD than at the anomalous GVD.

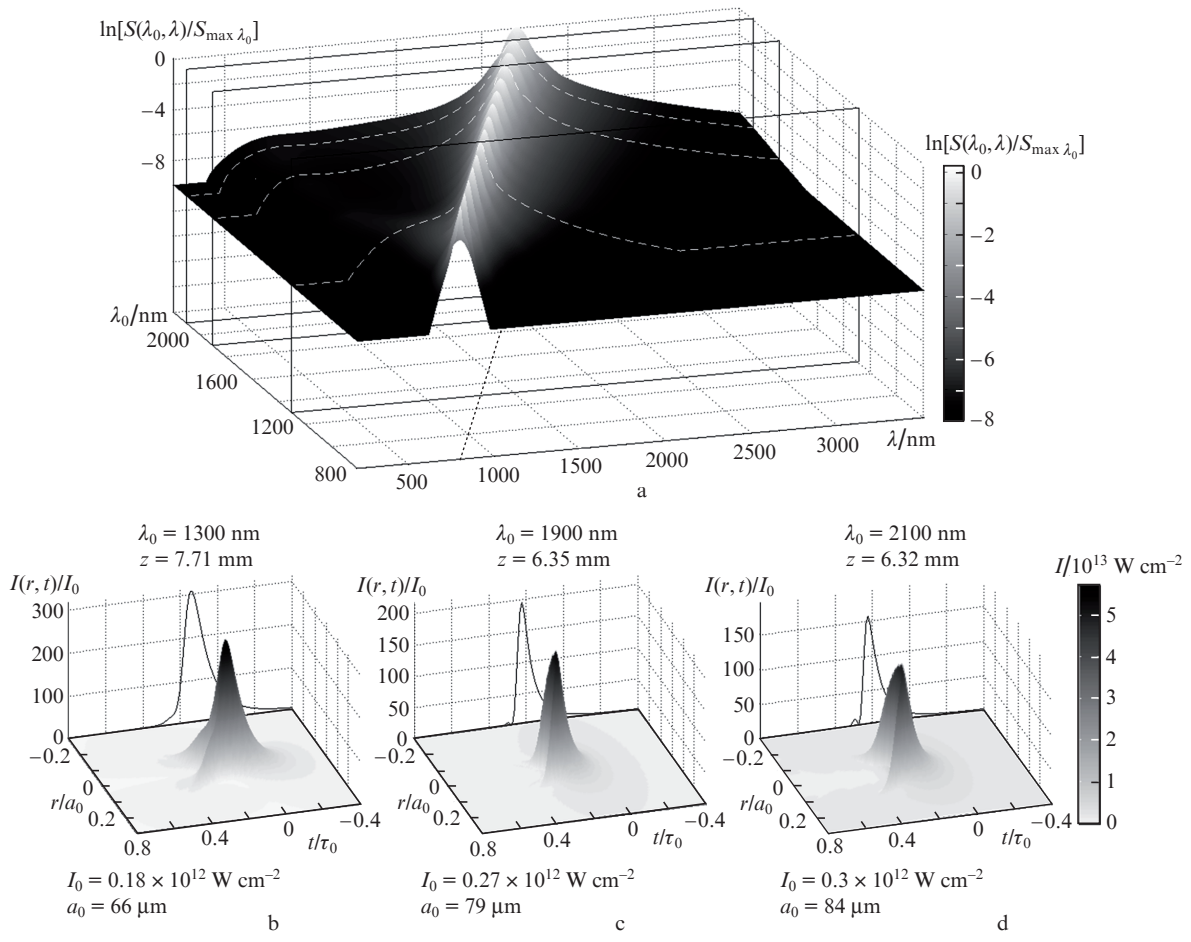


**Figure 2.** (a) Spectral map of the SC, $S_{comp}(\lambda_0, \lambda)$, for the wavelengths $\lambda_0 = 800–2300$ nm and (b–d) spatiotemporal intensity distributions, $I(r,t)$, for $\lambda_0 = 1300$, 1900 and 2100 nm at the nonlinear focus points.

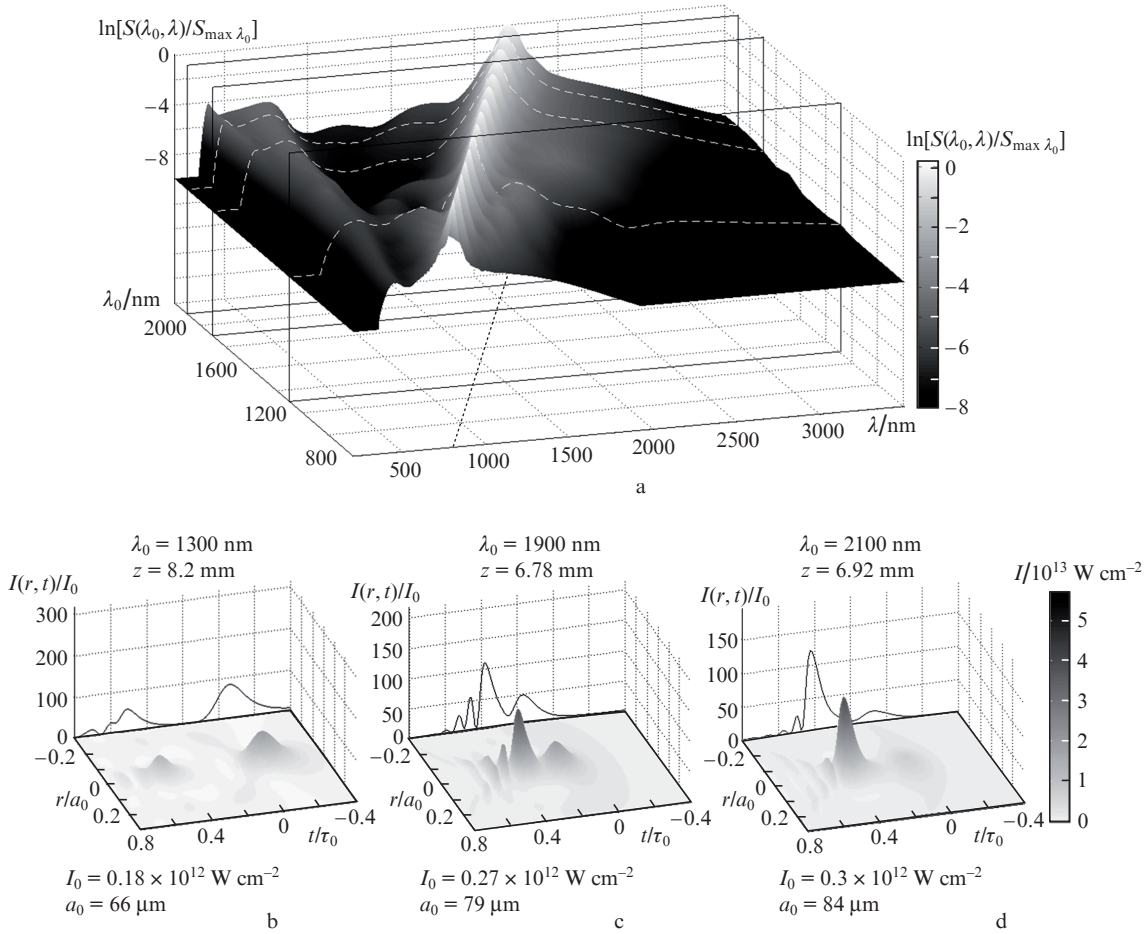


**Figure 3.** Same as in Fig. 2, with the length of the emitting region of ∼1 mm.

With increasing length of the emitting region, produced by the first light bullet in the filament, the SC spectrum changes qualitatively. The spectral map of the SC for the same length (∼1 mm) of the emitting regions is shown in Fig. 3. The SC spectra exhibit an additional modulation, which allows a clear separation of filamentation regimes in the case of the normal and zero GVD from the filamentation regime in the case of the anomalous GVD. At wavelengths $\lambda_0$ = 1400–2300 nm, lying in the region of the anomalous GVD, a clear broad minimum is formed in the anti-Stokes region of the SC, separating a monotonically broadened central part of the spectrum from the anti-Stokes wing of the spectral components in the range $\lambda$ = 600 nm. At the normal GVD, the depth of the spectrum modulation, $S_{comp}(\lambda)$, is small. The spatiotemporal distributions of the intensity $I(r,t)$ show that under conditions of the zero GVD, the pulse splits into subpulses, the intensity of which (for the propagation distance in question) is three times lower than the peak value in the nonlinear focus (Fig. 2). At the same time, the light bullet, which is formed under conditions of the anomalous GVD, is relatively stable and moves to the tail of the pulse, slowly decreasing in intensity. The shift of the light bullet is caused by the fact that it is a wave packet, whose spectrum is shifted to longer wavelengths from the centre wavelength $\lambda_0$, and its group velocity is less than that of the incident light. When the shift is significant, the light bullet disappears, and in the central time layers of the pulse, to which power 'contracts' due to the anomalous GVD, a new bullet is formed.

## 4. Radiation sources of the anti-Stokes wing of the SC

To determine the position of the anti-Stokes SC emission sources in the femtosecond pulse, the data of the numerical experiment were processed for for the pulse with the centre wavelengths $\lambda_0$ = 300 and 1900 nm. The results are shown in Fig. 4. Processing was performed for 1900-nm pulses at a distance $z$ = 6.35 mm, corresponding to the formation of a light bullets, and at $\lambda_0$ = 1300 nm at a distance $z$ = 7.71 mm, where the nonlinear focus emerged and a 'fish-like' spectrum, signature of filamentation at the zero GVD, was formed [8]. In the frequency-angular SC spectra $S(\theta,\lambda)$, the tone images of which are presented in Figs 4c, g, the SC spectra $S_{as}(\theta,\lambda)$ in the anti-Stokes band $\lambda$ = 400–1100 nm are shown (Figs 4d, h). The spatiotemporal intensity distributions of the anti-Stokes radiation, $I_{as}(r,t)$, obtained from its spectrum $S_{as}(\theta,\lambda)$ by the inverse Fourier transform, are presented by tone images on half-plane with the coordinates $r, t$ (Figs 4b, f). The pulse intensity distributions, $I(r,t)$, in the filament at the chosen distances are shown in Figs 4a, e. Comparison of the intensity distributions, $I_{as}(r,t)$ and $I(r,t)$, shows that the anti-Stokes SC emission sources are concentrated at the pulse tail in the region with the greatest slope of the trailing edge. To this end, these sources are located both on the axis of the beam, where their intensity is maximal, and on the trailing edge of the ring structures of the filament, where the temporal intensity gradients are significant.

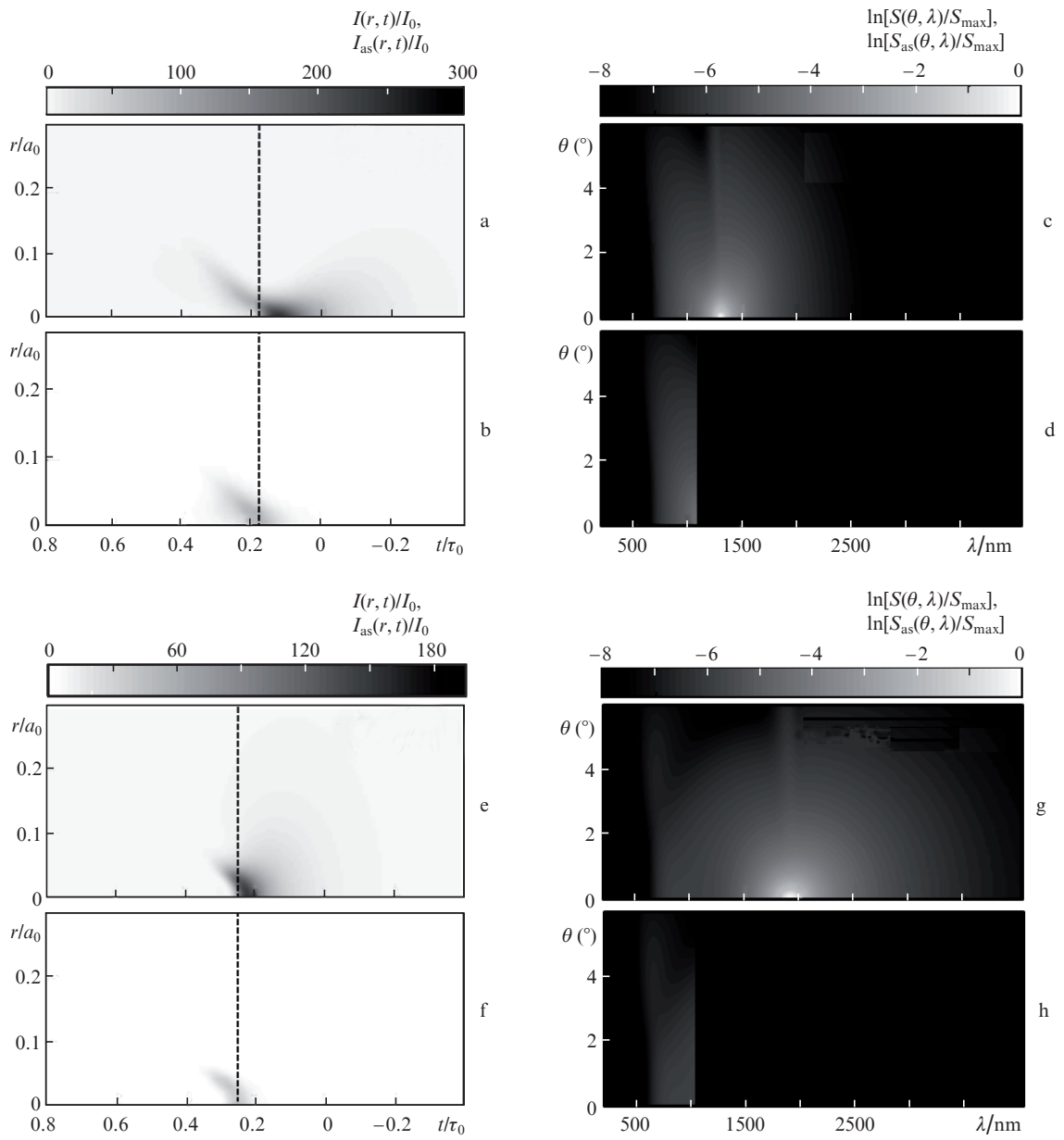


**Figure 4.** Spatiotemporal distributions of the radiation intensity $I(r,t)$ in the filament (a, e), the intensity $I_{as}(r,t)$ of the radiation sources in the anti-Stokes spectral band (b, f), as well as the frequency-angular SC spectra $S(\theta,\lambda)$ (c, g) at fixed distances $z$ = 7.71 and 6.35 mm upon filamentation of radiation with $\lambda_0$ = 1300 (a–d) and 1900 nm (e–h), respectively, in fused silica. Figures 4d and h demonstrate the anti-Stokes region of the frequency-angular spectrum $S_{as}(\theta,\lambda)$ at $\lambda$ = 400–1100 nm. The dashed line shows the time when the intensity of the anti-Stokes radiation sources is maximal.

## 5. Conclusions

Thus, in the case of femtosecond laser pulse filamentation under conditions of the anomalous GVD, a quasi-periodic sequence of light bullets with a strong spatiotemporal localisation of the light field is formed along the filament. The light bullet is produced in the central time layers of the pulse and moves towards the tail of the propagating pulse. The emergence of light bullets in the filament is directly related to the generation of plasma. When forming a light bullet, its spectrum monotonically broadens, and when the light bullet shifts to the pulse tails, an isolated anti-Stokes wing of the SC is produced.

In fused silica, with increasing centre wavelength and thus moving from the zero GVD ($\lambda_0$ = 1300 nm) to the anomalous GVD, the frequency-angular SC spectrum changes its shape from the 'fish-like' spectrum, characteristic of the zero GVD, to the 'O-shaped', which is typical of the anomalous GVD. However, under the conditions of the anomalous GVD, the spectrum contains divergent conical-emission components of the anti-Stokes wing of the SC. At a sufficiently long emitting region, the anti-Stokes wing is separated from the central 'O-shaped' part of the spectrum by a broad minimum. The shift of the isolated anti-Stokes wing to the blue region grows and its width becomes narrower with increasing pulse wavelength. At $\lambda_0$ = 1300 nm, which corresponds to the zero GVD, the ligth field is localised in space and time near the central time layers of the pulse, while at the pulse tail the ligth field is refocused. At $\lambda_0$ = 1900 and 2100 nm due to the power transfer from the tail and the front edge of the pulse to the centre, caused by the anomalous GVD, the conditions are created for the repeated formation of the light bullet, which eventually

leads to the formation of a sequence of bullets. At the distance of the formation of each bullet the SC spectrum monotonically broadens to the Stokes and anti-Stokes regions. Its shift to the pulse tail is accompanied by the formation of an isolated anti-Stokes wing of the SC. Radiation sources of the anti-Stokes SC components are located on the trailing edge of the pulse, the slope of which increases with increasing centre wavelength of the input pulse.

***Acknowledgements.*** This work was supported by the Russian Foundation for Basic Research (Grant Nos 11-02-00556a and 12-02-31690). Kompanets and Chekalin are grateful for the support of the scientific school headed by Prof. Vinogradov (Grant No. NSh-1049.2012.2). Research of Kandidov and Smetanina was supported by the Grant of the President of the Russian Federation for State Support of Leading Scientific Schools of the Russian Federation (Grant No. NSh-6897.2012.2) and by the grant of the Ministry of Education and Science of the Russian Federation (Grant No. 8393).

## References

1. Kandidov V.P., Kosareva O.G., Golubtsov I.S., Liu W., Becker A., Akozbek N., Bowden C.M., Chin S.L. *Appl. Phys. B*, **77**, 149 (2003).
2. Chin S.L., Hosseini S.A., Liu W., Luo Q., Theberge F., Akozbek N., Becker A., Kandidov V., Kosareva O., Schroeder H. *Can. J. Phys*., **83**, 863 (2005).
3. Couairon A., Mysyrowicz A. *Phys. Rep*., **441**, 47 (2007).
4. Kandidov V.P., Shlenov S.A., Kosareva O.G. *Kvantovaya Elektron*., **39**, 205 (2009) [*Quantum Electron*., **39**, 205 (2009)].
5. Bolonski I.V., Kadan V.N., Shpotyuk O.I., Dmitruk I.N., Pavlov I.A. *Pis'ma Zh. Eksp. Teor. Fiz*., **89**, 636 (2009).
6. Minardi S., Gopal A., Couairon A., Piskarskas R., Dubietis A., Di Trapani P. *Opt. Lett*., **34**, 3020 (2009).
7. Berge L., Skupin S. *Phys. Rev. E*, **71**, 065601(R) (2005).
8. Kandidov V.P., Smetanina E.O., Dormidonov A.E., Kompanets V.O., Chekalin S.V. *Zh. Eksp. Teor. Fiz*., **140**, 484 (2011).
9. Schrauth S.E., Shim B., Slepkov A.D., Vuong L.T., Gaeta A.L., Gavish N., Fibich G. *Opt. Express*, **19**, 9309 (2011).
10. Moll K.D., Gaeta A.L. *Opt. Lett.*, **29**, 995 (2004).
11. Bergé L., Mauger S., Skupin S. *Phys. Rev. A*, **81**, 013817 (2010).
12. Liu J., Li R., Xu Z. *Phys. Rev. A*, **74**, 043801 (2006).
13. Zheltikov A.M. *Usp. Fiz. Nauk*, **176**, 623 (2006).
14. Bondarenko N.G., Eremina B.V., Talanov V.I. *Pis'ma Zh. Eksp. Teor. Fiz*., **12**, 125 (1970).
15. Brodeur A., Chin S.L. *Phys. Rev. Lett*., **80**, 4406 (1998).
16. Naguro Ch., Suda A., Kawano H. *Appl. Opt*., **41**, 3735 (2002).
17. Liu W., Petit S., Becker A., et al. *Opt. Commun*., **202**, 189 (2002).
18. Nguyen N.T., Saliminia A., Liu W., Chin S.L., Vallée R. *Opt. Lett*., **28**, 1591 (2006).
19. Bradler M., Baum P., Riedle E. *Appl. Phys. B*, **97**, 561 (2009).
20. Dharmadhikari A.K., Rajgara F.A., Mathur D. *Appl. Phys. B*, **82**, 575 (2006).
21. Dachraoui H., Oberer C., Michelswirth M., Heinzmann U. *Phys. Rev. A*, **82**, 043820 (2010).
22. Saliminia A., Chin S.L., Vallée R. *Opt. Express*, **13**, 5731 (2005).
23. Naudeau M.L., Law R.J., Luk T.S., Nelson T.R., Cameron S.M. *Opt. Express*, **14**, 6194 (2006).
24. Brabec T., Krausz F. *Phys. Rev. Lett*., **78**, 3282 (1997).
25. Agrawal G.P. *Nonlinear Fiber Optics* (New York: Academic Press, 2007).
26. Akhmanov S.A., Vysloukh V.A., Chirkin A.S. *Optics of Femtosecond Laser Pulses* (New York: American Institute of Physics, 1992; Moscow: Nauka, 1988).
27. Stolen R.H., Gordon J.P., Tomlinson W.J., Haus H.A. *J. Opt. Soc. Am. B*, **6**, 1159 (1989).
28. Olivier T., Billard F., Akhouayri H. *Opt. Express*, **12**, 1377 (2004).
29. Keldysh L.V. *Zh. Eksp. Teor. Fiz*., **47**, 1945 (1964).
30. Smetanina E.O., Dormidonov A.E., Kompanets V.O. *Opt. Zh*., **7**, 75 (2010).